C21 preserves endothelial function in the thoracic aorta from DIO mice: role for AT_2, Mas and B_2 receptors

Raquel González-Blázquez[1], Martín Alcalá[2], María S. Fernández-Alfonso[3,4], Ulrike Muscha Steckelings[5], M Paz Lorenzo[2], Marta Viana[2], William A. Boisvert[6,7], Thomas Unger[8], Marta Gil-Ortega[1]* and Beatriz Somoza[1]*

[1]Departamento de Ciencias Farmacéuticas y de la Salud, Facultad de Farmacia, Universidad San Pablo-CEU, CEU Universities, 28925, Madrid, Spain. [2]Departamento de Química y Bioquímica, Facultad de Farmacia, Universidad CEU-San Pablo, CEU Universities, 28925, Madrid, Spain. [3]Instituto Pluridisciplinar, Unidad de Cartografía Cerebral, Universidad Complutense de Madrid, 28040 Madrid, Spain. [4]Departamento de Farmacología, Facultad de Farmacia, Universidad Complutense de Madrid, 28040 Madrid, Spain. [5]Department of Cardiovascular and Renal Research, Institute of Molecular Medicine, University of Southern Denmark, Odense, Denmark. [6]Center for Cardiovascular Research, John A. Burns School of Medicine, University of Hawaii, 651 Ilalo Street, BSB311, Honolulu, HI 96813, USA. [7]Institute of Fundamental Medicine and Biology, Kazan Federal University, 18 Kremlevskaya Str., Kazan 420008, Russia. [8]CARIM - School for Cardiovascular Diseases, Maastricht University, Maastricht, The Netherlands.

* These authors contributed equally to this work.

Short title: C21 and endothelial function: AT_2/Mas/B_2K crosstalk

Corresponding author:

Marta Gil Ortega

Universidad CEU San Pablo, Facultad de Farmacia

Ctra. Boadilla del Monte Km 5.300, 28925, Alcorcón, Madrid (Spain)

Telephone number: (+34) 913724700

Fax number: (+34) 913724775

e-mail address: mgortega@ceu.es

ABSTRACT

Compound 21 (C21), a selective agonist of angiotensin type 2 receptor (AT_2R), induces vasodilation through NO release. Since AT_2R seems to be overexpressed in obesity, we hypothesize that C21 prevents the development of obesity-related vascular alterations. The main goal of this study was to assess the effect of C21on thoracic aorta endothelial function in a model of diet-induced obesity and to elucidate the potential crosstalk between AT_2R, MasR and/or B_2R in this response.

5-week-old male C57BL6J mice were fed a standard (CHOW) or a high-fat diet (HF) for 6 weeks and treated daily with C21 (1mg/Kg p.o) or vehicle, generating four groups: CHOW-C, CHOW-C21, HF-C, HF-C21. Vascular reactivity experiments were performed in thoracic aorta rings. Human endothelial cells (EA.hy926) were used to elucidate the signaling pathways, both at receptor and intracellular levels.

Arteries from HF mice exhibited increased contractions to Ang II than CHOW mice, effect that was prevented by C21. PD123177, A779 and HOE-140 (AT_2R, Mas and B_2R antagonists) significantly enhanced Ang II-induced contractions in CHOW but not in HF-C rings, suggesting a lack of functionality of those receptors in obesity. C21 prevented those alterations and favoured the formation of AT_2R/MasR and MasR/B_2R heterodimers. HF mice also exhibited impaired relaxations to acetylcholine due to a reduced NO availability. C21 preserved NO release through PKA/p-eNOS and AKT/p-eNOS signaling pathways.

In conclusion, C21 favours the interaction between AT_2R, MasR and B_2R and prevents the development of obesity-induced endothelial dysfunction by stimulating NO release through PKA/p-eNOS and AKT/p-eNOS signaling pathways.

KEYWORDS: Compound 21, nitric oxide, angiotensin II type 2 receptor, Mas receptor, bradykinin type 2 receptor, diet-induced obesity.

NON-STANDARD ABBREVIATIONS AND ACRONYMS: ACh: acetylcholine; Ang: angiotensin; AT_1R: angiotensin II type 1 receptor; AT_2R: angiotensin II type 2 receptor; BK: bradykinin: B_2R; bradykinin type 2 receptor; BW: body weight; C21: Compound 21; DIO: diet-induced obesity; HECs: human endothelial cells; HFD: high-fat diet; MasR: Mas receptor; Phe: phenylephrine.

1. INTRODUCTION

Obesity has reached epidemic dimensions and is nowadays a major public health concern. Affecting more than 1 billion people worldwide, obesity is directly connected to cardiovascular diseases which comprise the two major causes of death in the world, ischemic heart diseases and stroke [1]. Pathological conditions shared in the etiology of these diseases are vascular alterations including endothelial dysfunction, decreased vascular compliance and reduced blood flow, among others [2]. In this context, our group and others have demonstrated the deleterious effects of HFD intake and human morbid obesity on vascular disorders such as arterial stiffness and endothelial dysfunction associated with a reduced NO availability and AMPK activity together with an increase in oxidative stress [3–7].

The renin-angiotensin system [RAS, extensively reviewed in [8,9]] plays a key role in the regulation of cardiac and vascular functions. It includes a network of enzymes, bioactive peptides and receptors that systemically participate in the control of blood pressure and vascular homeostasis. The precursor, angiotensinogen, an inactive protein secreted mainly by the liver and the adipose tissue [10], is sequentially transformed into numerous oligopeptides with differential biological functions. Among them, angiotensin II (Ang II) mediates the classical cardiovascular and renal effects. It interacts with Ang II type 1 receptor (AT_1R) and Ang II type 2 receptor (AT_2R), both G protein-coupled receptors (GPCR). The AT_1R is expressed ubiquitously and its activation leads to increase in blood pressure by promoting vasoconstriction, water and Na^+ retention [11], as well as oxidative stress [12], inflammation, cardiac hypertrophy [13] or fibrosis [14], among others. AT_2R is ubiquitously expressed in human fetal tissues, but its expression rapidly declines after birth. Although AT_2R level in adults is typically low, its expression rises in pathophysiological situations such as diabetes, inflammation, hypertension and

atherosclerosis [15]. Its activation promotes the activity of phosphotyrosine phosphatases [DUSP1/ MKP-1, PP2A and SHP-1] and stimulates NO generation, which counteracts the pathological effects of AT_1R by inducing vasodilation, reducing fibrosis and inflammation, among others [16].

Beyond these classic interpretations, new receptors (AT_4R/IRAP, Mas receptor, renin/prorenin receptor or the Mas-related G-protein coupled receptor type D), as well as relaxant (Ang 1-7, Ang 1-9, Alamandin) and contractile peptides (Ang III, Ang IV) have been reported to participate in a tightly regulated mechanism to control blood pressure [17].

The regulatory negative crosstalk between AT_2R and AT_1R is critical for the proper functioning of the vascular system. Ang II-induced AT_1R expression and its vascular effects are boosted in AT_2R KO animals [18]. On the other hand, Ang II administration in the presence of AT_1R blockers mediate AT_2R-dependent aortic relaxation [19]. Furthermore, AT_2R activation and overexpression inhibit AT_1R expression in an NO-dependent manner [20]. In addition to these functional relations, a physical interaction between the two receptors has been described. Indeed, AT_1R-AT_2R heterodimers regulate the internalization and the signaling pathways of both receptors both in ligand dependent [21] and independent fashion [22]. Similarly, AT_2R might heterodimerize with MasR [23] and with bradykinin (BK) receptor (B_2R) [24], leading to a synergistic potentiation of the phosphatase activity and NO/cGMP production and reinforcing its vasodilatory actions. Highlighting the relevance of this combined signaling, the activation of downstream markers of AT_2R was increased after the treatment with the AT_2R selective agonist, C21, but depleted when the antagonist of the MasR was simultaneously used. The same effect was observed when an agonist of the MasR and

an antagonist of the AT_2R were concomitantly used [23]. Similarly, NO release in response to AT_2R activation was blunted in presence of a B_2R antagonist [25].

In obesity, the circulating levels of members of the "deleterious arm" of the RAS (angiotensinogen, Ang I, ACE, Ang II) are increased partially due to a strong contribution of secretion from the white adipose tissue [26]. Local expression of AT_1R and renin/prorenin receptors is also increased [27], which may account for obesity-related hypertension and cardiovascular dysfunction. However, although the elements of the "protective arm" are supposed to be activated under pathological stress [28], there is limited evidence of the upregulation and activation of these pathways in obesity at a vascular level. To the best of our knowledge, in obesity there are no reports about vascular expression of MasR and only a slight increase in the protein levels of AT_2R has been reported in mesenteric arteries from monosodium-glutamate fed obese rats [29] and abdominal arteries of HFD obese rats [30].

The goal of the present study was to analyze the effects of AT_2R activation on thoracic aorta endothelial function in a model of diet-induced obesity using the specific agonist C21. Our hypothesis was that obesity promotes a state of resistance to the beneficial effects of the protective arm of the RAS by disrupting the AT_2R-MasR-B_2R interaction and BK/NO/cGMP pathways. We show that the activation of AT_2R with C21 could prevent obesity induced impairment of signaling and function of the protective RAS thus preserving endothelial function.

2. METHODS

2.1. Animal model

All experiments were performed in four-week old male C57BL/6J mice, from Charles River strains and inbred at Universidad San Pablo-CEU animal facilities and housed under controlled light (12:12 h light-dark cycles), temperature (22-24 °C) and relative

humidity (44-55%) with standard food and water *ad libitum* and placed in individual cages. After one week of acclimation, animals with similar average body weight (BW) were divided into two groups and assigned to a control CHOW diet (CHOW) or to a high-fat diet (HF). CHOW diet (Teklad Rodent Diet 2918, 18 % of Kcal from fat, 58 % of Kcal from carbohydrates and 24 % of Kcal from proteins; 3.1 kcal/g) was supplied by Envigo (USA) and HF diet (D12451, 62 % of Kcal from fat, 20 % of Kcal from carbohydrates, and 18 % of Kcal from proteins; 5.1 kcal/g) was supplied by Test Diet (UK). All animals had free access to food for 6 weeks. Simultaneously, half of the animals of each group were treated with Compound 21 (C21; 1 mg/kg/day in drinking water), thus generating 4 different groups CHOW-C, CHOW-C21, HF-C, HF-C21.

Both BW and food intake were monitored twice a week. Water intake was monitored daily. Energy consumption was calculated from food intake values and expressed as Kcal/day/mice. Caloric efficiency was calculated from BW increase/Kcal intake per animal per week and expressed as g/Kcal. On the last day, mice were weighed and euthanized by decapitation at 9 am under inhalational anesthesia with isoflurane (5%). Thoracic aorta was immediately removed and used for vascular function studies. Blood was collected in chilled heparin-coated polypropylene tubes, centrifuged at 800G for 20 min to obtain the plasma, which was stored at -80ºC until biochemical analysis.

All experimental procedures were performed in accordance the Directive 2010/63/EU of the European Parliament on the protection of animals used for scientific purposes and were approved by the Animal Research Committee of San Pablo CEU University (PROEX 200/18).

2.2. Plasma measurements

Insulin was determined by means of a specific ELISA kit for mouse insulin (Mercodia, Denmark) (2.2% intra-assay variation, 4.9% inter-assay variation). Glucose (glucose

Trinder Method, Roche Applied Science, Barcelona, Spain), triglycerides (glycerol phosphate oxidase method, Biolabo, Maizy, France), non-esterified fatty acids (Acyl-CoA oxidase method, Wako, Bioproducts, Germany) and cholesterol (cholesterol oxidase - peroxidase method, Spinreact, Barcelona, Spain) were measured by enzymatic colorimetric methods.

2.3. Functional studies in the thoracic aorta

Thoracic aortas were carefully dissected, placed in cold Krebs buffer solution, cleaned of perivascular adipose tissue, cut into 2-3-mm length rings and introduced in an organ bath as previously described [31]. Isometric tension was recorded in a Power Lab system (ADInstruments, Oxford, UK). Aortic segments were given an optimal resting tension of 1 g. After 40 min of equilibration period, arterial contractility was assessed with potassium chloride (KCl, 60 mmol/l). Endothelial integrity was analyzed with acetylcholine (ACh, 10^{-9}-10^{-4} mol/l) on aortic segments pre-contracted with a submaximal concentration of phenylephrine (Phe, 10^{-6} mol/l). Cumulative concentration-response curves to Ang II (10^{-9}-10^{-6} mol/l) were carried out to analyze the contractile response to Ang II. In addition, relaxations curves to Ang II (10^{-9}-10^{-6} mol/l) were also performed in segments pre-contracted with Phe (10^{-6} mol/l) and preincubated with Losartan (AT_1R antagonist, 10^{-7} mol/l, 20 min) to block the contractile response elicited by Ang II through this receptor. Some aortic rings were preincubated for 20 min with NG-nitro-L-arginine methyl ester (L-NAME, NOS inhibitor, 10^{-4} mol/l), PD123177 (AT_2R antagonist, 10^{-7} mol/l), HOE-140 (B_2R antagonist, 10^{-7} mol/l), KT-5720 (PKA inhibitor, 10^{-5} mol/l) or triciribine (AKT inhibitor, 10^{-5} mol/l) or for 5 min with A779 (MasR antagonist, 10^{-6} mol/l) before adding the agonists. All the reagents were provided by Sigma-Aldrich (Spain).

2.4. Functional studies data analyses

Contractile responses to Ang II are expressed as percentage of maximal contraction to KCl. Relaxations are expressed as percentage of contraction to Phe. The maximal response (E_{max}) and the potency (pD_2) of ACh or Ang II were determined by a non-linear regression analysis of each individual concentration-response curve. Area under the concentration-response curves (AUC) were calculated from the individual concentration response curve plots (GraphPad Software, California, United States).

2.5. Cell culture experiments

Human umbilical vein endothelial cells (cell line EA.hy926, HECs) were obtained from the American Type Culture Collection (ATCC). HECs were cultured in DMEM high-glucose with L-glutamine (2 mmol/l), 10% FBS (Biowest, USA), penicillin (100 U/mL) and streptomycin (100 μg/mL) (Lonza, Switzerland) and maintained at 37ºC in a humidified atmosphere containing 5% CO_2. Sub-confluent HECs were serum-starved for 4h. To study the role of AT_2, B_2 and Mas receptors in C21-induced NO production, HECs were treated either with C21 alone (10^{-6} mol/l,5 min) or in combination with the respective antagonists PD123177 (10^{-7} mol/l, 20 min), A779 (10^{-6} mol/l,5 min) or HOE-140 (10^{-7} mol/l, 20 min), with which cells were pretreated for the indicated periods of time.

BK and Ang 1-7 concentrations were determined in cell culture media from HECs incubated or not with C21 (10^{-6} mol/l, 5 min) by using a specific enzyme immunoassay commercial kit (Cloud-Clone Corp. S.L. USA; CV<10% intra-assay variation, CV<12% inter-assay variation).

To assess the involvement of PKA and AKT signaling pathways, KT-5720 (10^{-5}mol/l, 20 min), triciribine (10^{-5} mol/l, 20 min) or a combination of both KT-5720+triciribine treatments were performed prior to a 5 min incubation with C21 (10^{-6} mol/l).

2.6. Western blot studies

Western blot experiments were performed in HECs as previously described [32]. 1.2 x 10^5 cells/well were seeded in a 6-well plate and grown to 90% confluence. HECs, which had been treated as described in the previous section, were washed with ice-cold PBS and scraped in lysis buffer containing (50 mmol/l $Na_4P_2O_7$, 50 mmol/l NaF, 5 mmol/l EDTA, 5 mmol/l NaCl, 5 mmol/l EGTA, 10 mmol/l HEPES, 0,5 % Triton X-100, 2mmol/l phenylmethylsulfonyl fuoride, 1 µl/ ml leupeptin, 1µl/ml aprotinin, and 0.5µl/ml Tosyl-L-lysyl-chloromethane hydrochloride). Cell lysates were centrifuged at 18000G for 20 min at 4 °C. Protein concentrations were determined in the supernatants with the BCA reagent. 30 µg protein samples were loaded in Laemmli buffer [50 mmol/l Tris (pH 6.8), 10% sodium dodecyl sulfate, 10% glycerol, 5% mercaptoethanol, and 2 mg/ml blue bromophenol] and size-separated in 7%-10% SDS-PAGE. Proteins were transferred to nitrocellulose (Bio-Rad, Hercules, CA) using a transblot apparatus (Bio-Rad, Hercules, CA). For immunoblotting, membranes were blocked with 5% nonfat dried milk for 1h. Primary antibodies against p-eNOS (Ser^{1177}) (1:500 dilution; Cell Signaling Technology, USA), eNOS (1:500 dilution; BD Transduction Laboratories, UK), AT_2R (1:1000 dilution; Abcam, Germany), MasR (1:10000 dilution; Abcam, Germany) and B_2R (1:500 dilution, Santa Cruz Biotechnology, USA) were applied overnight at 4ºC. After washing, appropriate secondary antibodies (anti-rabbit or anti-mouse IgG-peroxidase conjugated; 1:2000 dilution) were applied for 1h. Blots were washed, incubated in enhanced chemiluminescence reagents (ECL Prime, Amersham Bioscence, UK) and bands were detected by ChemiDoc XRS+ Imaging System (Bio-Rad, USA). To prove equal loadings of samples, blots were re-incubated with α-tubulin antibody (1:1000 dilution; Cell Signaling Technology, Massachusetts,

USA) or β-actin antibody (1:5000 dilution; Sigma-Aldrich, Spain). Blots were quantified using Image Lab 6.0 software (Bio-Rad, USA).

2.7. Co-immunoprecipitation

1.5 x 10^{6} cells were seeded in a 10 cm-diameter Petri dish and grown to 90% confluence. HECs were serum-fasted for 4h, treated with C21 (10^{-6} mol/l, 5 min) and crosslinked with 3,3′-dithiodipropionic acid (N-hydroxysuccinimide ester) (DSP, 2 mmol/l; Sigma-Aldrich, Spain) for 30 min. After quenching the crosslinker with Tris (20 mmol/l) pH 7.4 in PBS with $Ca^{2+}$and Mg^{2+} (D-PBS) (Thermo, USA), HECs were lysed in lysis buffer (50 mmol/l $Na_4P_2O_7$, 50 mmol/l NaF, 5 mmol/l EDTA, 5 mmol/l NaCl, 5 mmol/l EGTA, 10 mmol/l HEPES, 0,5 % Triton X-100) with protease inhibitors at 4ºC for 45 min. Protein concentrations of the lysates were determined using the BCA reagent and 1.5 mg of protein were incubated overnight at 4ºC with 2 µg of rabbit anti-Mas antibody (Abcam, Germany). The immunocomplex was subsequently captured with 20 µl of prewashed protein A/G PLUS-Agarose beads (Santa Cruz Biotechnologies, USA) overnight at 4ºC. Immunoprecipitants were then washed 3 times with washing buffer (50 mmol/l HEPES, 0.1% Nonidet P-40, 5 mmol/l EDTA 250 mmol/l NaCl, protease inhibitor cocktail, pH = 8) and re-suspended in Laemmli buffer to a final volume of 30 µl. Samples were resolved by SDS-PAGE as aforementioned, followed by immunoblotting analysis using rabbit anti-Mas (1:10000 dilution; Abcam, Germany), rabbit anti-AT_2R (1:1000 dilution; Abcam, Germany), mouse anti-B_2R (1:500 dilution; Santa Cruz Biotechnologies, USA) and rabbit anti-α-tubulin (1:1000 dilution; Cell Signaling, USA) as a Co-IP specify control. Input protein samples were loaded along with the Co-IP samples, washing supernatants and positive controls. Non-conjugated beads were loaded as negative controls. Images were analyzed using Image

Lab 6.0 software (Bio-Rad, USA). IP bands were normalized by their corresponding input signals and expressed relative to control.

2.8. Co-localization studies

The interaction between AT_2, Mas and B_2 receptors was assessed in HECs by immunofluorescence. 2 x 10^4 cells/well were seeded in coverslips in a 24 well plate and grown to 70% confluence, fasted for 4h and treated with C21 (10^{-6} mol/l, 5 min) and fixed in 4% paraformaldehyde (PFA, in D-PBS for 15 min at room temperature, RT). Briefly, HECs were incubated with anti-AT_2 (1:50; Santa Cruz Biotechnologies, USA), Mas (1:100; Abcam, Germany) or B_2 (1:50 dilution; Abcam, Germany) receptors antibodies overnight at 4ºC. HECs were washed and incubated with Alexa Fluor 555® or Alexa Fluor 488® anti-rabbit IgG and anti-mouse IgG, respectively (1:200 dilution, Invitrogen, USA) for 1h at RT in the darkness. Afterwards, nuclei were stained with DAPI (1:500, 10 min, RT, Molecular Probes, USA). Fluorescence analysis was performed at 63x zoom 3 using a confocal microscope (SP5 Leica Microsystems, Germany). Cells incubated only with secondary antibody were used as negative control. "Co-localization analyses were performed by using the ICA (Intensity Correlation Analysis; http://www.uhnresearch.ca/facilities/wcif/imagej/colour_analysis.htm) plugging as described by Li *et al.* 2004 [33]. The Pearson correlation coefficient (PCC) and the Mander's overlap coefficient (MOC) were determined to quantify the degree of co-localization between AT_2R and MasR or B_2R."

2.9. In vitro NO production

Sub-confluent HECs, previously serum-fasted for 4h, were treated with C21 (10^{-6} mol/l, 5 min) in cells previously treated with PD123177 (10^{-7} mol/l, 20 min), A779 (10^{-6} mol/l,

5 min), HOE-140 (10^{-7} mol/l, 20 min), KT-5720 (10^{-5} mol/l, 20 min), triciribine (10^{-5} mol/l, 20 min) or both KT-5720+triciribine. Thereafter, to assess NO production, treated HECs were incubated with 4,5-diaminofluorescein diacetate (DAF-2 DA, 10^{-5} mol/l; Sigma-Aldrich, USA) for 30 min at 37ºC in the dark, nuclei were stained with DAPI (1/5000; Molecular Probes, USA) and HECs were fixed in 4% PFA. The cover slips were mounted in a glycerol/PBS solution (Citifluor, VWR International, Spain) and analyzed with a fluorescence microscope (DM5500B, Leica, Solms, Germany). From each culture, a minimum of 2 randomly selected images were captured using the 488nm/530nm (DAF-2DA, NO) and 405nm/410–475nm (DAPI, nuclei) filters with a x20 objective. To ensure the selection of complete cells in the acquired field, cells with an area of >400 μm^2 were analyzed using the "Analyze Particle" function in ImageJ software (NIH, Bethesda, MD, Version 1.50f). After applying the threshold, mean fluorescence signal per cell was calculated.

2.10. Chemicals

ACh and L-NAME were dissolved in saline, Phe in 0.01% ascorbic acid/saline and Ang II, A779, Losartan, HOE-140 and C21 in distilled water. Triciribine was dissolved in DMSO and KT-5720 in methanol. All reagents were purchased from Sigma-Aldrich (USA) with the exception of C21 that was provided by Vicore Pharma.

2.11. Statistical analysis

Results are expressed as mean ± SEM and n denote the number of animals used in each experiment. Comparison between groups were made by performing a Student's t-test, one or two-way analysis of variance (ANOVA) as appropriate using GraphPad Prism 07 (San Diego, CA, USA). Post-hoc comparisons were carried out with Bonferroni´s test. Statistical significance was set at $p<0.05$.

3. RESULTS

3.1. Effect of HF-feeding and C21 treatment on BW, biochemical parameters and RAS components

Mice fed the HF diet exhibited a significant increase in both BW and energy intake together with a reduction in water intake that were not modified by the treatment with C21 (Supplemental Figure 1 and Table 1). Plasma levels of glucose, insulin and cholesterol were significantly higher in the HF group. The treatment with C21 only reduced insulin and NEFA levels in HF mice, without modifying neither glucose nor cholesterol levels (Table 1).

3.2. C21 reverses HF-induced alterations in both contractile and relaxant responses to Ang II through the activation of AT_2R, MasR and B_2R receptors

In a first set of experiments, we aimed to evaluate the impact of a 6-week HF diet and the effect of C21 treatment on vascular responses to Ang II. Previously, we assessed the maximal contractile ability of the thoracic aorta segments to KCl (60 mM), without finding differences between groups (Supplemental table 1). Compared to the CHOW mice, contractions to Ang II (10^{-9}-10^{-6} mol/l; Figure 1A) were significantly increased in aortas from HF mice affecting both the maximal response (E_{max}) and AUC values but not the potency (PD_2) (Supplemental Table 2). Treatment with C21 reduced contractions to Ang II to similar values than the CHOW group (Supplemental Table 2). To assess the participation of AT_2R, MasR and B_2R in this response, cumulative concentrations of Ang II (10^{-9} to 10^{-6}mol/l) were added to aortic rings previously incubated with the respective, specific antagonists PD123177, A779, and HOE-140, respectively. All antagonists significantly enhanced Ang II-induced contraction in

arteries from CHOW (Figure 1B, Supplemental Table 2); however, none of the inhibitors modified the contractile effect of Ang II in HF mice (Figure 1D and Supplemental Table 1) suggesting that HF diet abolishes the attenuation of Ang II-induced responses by AT_2R, MasR and B_2R. Interestingly, HF animals treated with C21 exhibited similar responses to the inhibitors as seen in CHOW mice (Figure 1E), indicating that C21 restores AT_2R, MasR and B_2R function in obese mice. No effect of C21 was observed in CHOW mice (Figure 1C, Supplemental Table 2).

We next analyzed the specific contribution of the AT_2R to relaxant responses to Ang II (10^{-9} to 10^{-6} mol/l) in rings preincubated with losartan (10^{-7} mol/l) and pre-constricted with Phe (1 μM). Phe-induced contractile responses were similar in all groups (Supplemental table 1). As shown in Figure 1F, Ang II-induced relaxation was nearly abolished by HF feeding (E_{max}; Supplemental Table 3) but restored by treatment with C21 in HF mice. Moreover, preincubation with PD123177, A779 or HOE-140 significantly inhibited the relaxation to Ang II (E_{max}) in both CHOW-C and in HF-C21 mice (Figures 1G and 1J, respectively and Supplemental Table 3) but not in HF-C mice (Figure 1I).

The differences in the AUC in absence or presence of PD123177, A779 or HOE-140, which indirectly indicate the contribution of the respective receptor, were significantly higher in HF-C21 mice than in HF-C mice for both contractile and relaxant responses to Ang II for all three antagonists (Supplemental Tables 2 and 3, respectively).

Altogether, these results suggest that there is a functional interaction between AT_2R, MasR and B_2R that is required for Ang II-mediated contractile and relaxant responses which is lost in HF mice but restored by the treatment with C21. The treatment with C21 did not modify vascular responses in CHOW mice (Figure 1H).

3.3. Ang II-induced relaxation through the activation of the AT_2R requires the association with both the MasR and B_2R

To better understand the interaction between AT_2R, MasR and B_2R, we performed co-immunoprecipitation studies of the three receptors in HECs. When the MasR was immunoprecipitated, simultaneous presence of both AT_2R and B_2R was detected, confirming an association between the three receptors. In addition, this interaction was significantly enhanced by the treatment with C21, as demonstrated by the increased co-IP/input ratio in the AT_2R and the B_2R (Figure 2B).

Immunofluorescent staining revealed that AT_2R is located mainly in the cell membrane, cytoplasm and perinuclear regions, while MasR is found mostly in the cytoplasm and, to a lesser extent, in the membrane of the HECs. The treatment with C21 increased the fluorescent signal of both receptors, with a stronger signal in the cellular membranes that become evident when the images are merged (Figures 2D, 2F and 2G).

B_2R staining is seen in the cytoplasm and the membrane in basal conditions, but its colocalization with AT_2R is weak (Figure 2E). Whereas treatment with C21 enhanced the fluorescence signal of B_2R in the cell membrane, there was a marked increase in the expression of B_2R in the perinuclear region and also in the nucleus (Figure 2E and 2H). Colocalization analyses revealed a similar overlapping ratio between AT_2R and both MasR and B_2R as evidenced by PCC and MOC (Table 2). However, since C21 increased AT_2R, MasR and B_2R protein amounts, the net colocalization rate between AT_2R/MasR and AT_2R/B_2R was higher in C21-treated cells than in control cells. Together, those data provide further evidence of the association amongst the three receptors.

Furthermore, HECs treated with C21 showed a significant increase in AT_2R, MasR and the glycosylated isoform of B_2R (Supplemental Figure 2). Altogether, these data corroborate the interaction amongst the AT_2, Mas and B_2 receptors in C21-mediated effects.

Finally, to elucidate whether C21 might induce a local production of BK or Ang 1-7, we analyzed the levels of both peptides in cell culture media after incubation with C21 (10^{-6} mol/l,5 min). BK levels were 2-fold higher in HECs treated with C21 (C=3.7 ± 0.7 µg/ml *vs* C21= 8.1± 1.1 µg/ml, $p<0.01$). However, Ang 1-7 was not detected in any experimental group.

3.4. C21 improves endothelial function in HF mice by increasing NO availability

To assess the impact of AT_2R stimulation on endothelial function in HF mice, we assessed concentration-dependent relaxations to ACh (10^{-9} to 10^{-4} mol/l). HF mice exhibited a significant impairment in endothelial-dependent relaxation to ACh and a reduction in E_{max} values as compared with CHOW animals ($E_{max\ CHOW-C}$= 85,6 ± 1,7% *vs* $E_{max\ HF-C}$= 63,8 ± 3,0%; two-way ANOVA, $p<0.001$, Figure 3A and Supplemental Table 4). Treatment with C21 prevented the development of endothelial dysfunction in HF mice ($E_{max\ HF-C21}$= 86,0 ± 1,8%, $p<0.001$ *vs* HF-C). The contribution of NO to endothelial function was assessed in the presence of L-NAME (10^{-4} mol/l), which abolished ACh-induced relaxations in all groups (Figures 3B-3E). However, NO availability, estimated from the difference in the AUC with or without L-NAME, was significantly reduced by the HF diet but preserved by the treatment with C21 (Figure 3F and Supplemental Table 4).

The molecular mechanism of C21 to prevent vascular dysfunction in HF-animals was analyzed in HECs. Stimulation of AT_2R by C21 enhanced eNOS phosphorylation at Ser^{1177}, which was completely blocked by PD123177, A779 or HOE-140 (Figure 4A). Similarly, NO availability (determined by DAF-2DA staining) was significantly augmented by the treatment with C21, but blunted by PD123177, A779 and HOE-140 (Figures 4B and 4C).

3.5. The activation of AT_2R by C21 enhances NO release through both PKA/p-eNOS and AKT/p-eNOS signaling pathways.

To better elucidate the mechanisms by which C21 was able to increase NO release in HF mice, we analyzed Ang II-induced relaxation (10^{-9} to 10^{-6} mol/l) in presence of either a selective inhibitor of the PKA (KT-5720, 10^{-5} mol/l) or an inhibitor of AKT phosphorylation (triciribine, 10^{-5} mol/l). Both KT-5720 and triciribine significantly reduced the relaxation to Ang II in CHOW animals, thus suggesting that both PKA/p-eNOS and AKT/p-eNOS signaling pathways are involved in Ang II-induced relaxation through the AT_2R. C21 treatment of mice *per se* did not result in any changes to the relaxant responses to Ang II in CHOW animals, as their arteries showed similar responses regardless of the presence or absence of the inhibitors (Figure 5B). In contrast, relaxant responses to Ang II were hardly absent in arteries from HF fed-animals and consequently also did not show any response to KT-5720 or triciribine preincubation (Figure 5C-5F). This corroborates the finding that the relaxant responses mediated by the AT_2R are absent in obese mice. However, when treated with C21, arteries from HF mice showed a recovery of the relaxant, AT_2R-mediated responses to Ang II through both a PKA and AKT-dependent mechanisms, since the pre-incubation with either KT-5720 or triciribine abrogated Ang II-induced relaxation (Figure 5D). These observations are further supported by the analysis of the AUC, which shows that

both PKA and AKT are responsible for NO synthesis and thus accounting for relaxant responses in both control and HF-C21 animals (Figure 5E and 5F).

Finally, we assessed NO release in HECs treated with C21 and preincubated with KT-5720 and/or triciribine. As expected, NO release was 5-fold higher in cells treated with C21 than in control cells (Figure 6A and 6B). Interestingly, while preincubation with either KT-5720 or triciribine only partially reduced C21-induced NO release, simultaneous treatment with both inhibitors completely blocked the C21-induced NO production, strongly indicating that AKT and PKA pathways contribute similarly to the NO production stimulated by C21.

4. DISCUSSION

Many reports have implicated the activation of the "deleterious arm" of the RAS in obesity-related endothelial dysfunction [26,27,34,35]. According to the conventional view of the RAS, the "protective arm" should be triggered in a pathological state such as obesity as a response to the negative effects driven by AT_1R activation. However, there is a general paucity of detailed information in the literature on the effects of triggering AT_2R or MasR pathways regarding vascular pathology in obesity, although pharmacological activation of these receptors has shown beneficial effects at metabolic and vascular levels [36,37]. We hypothesized that obesity leads to a miscommunication in the "protective arm" of the RAS that impedes the counteracting role of the AT_2R, B_2R and MasR pathways. If proven true, potentiating the effect of these pathways could protect the vascular system from the negative effects of obesity. To test this hypothesis, we have used a HFD-induced mouse obesity model to analyze the effects of the activation of the AT_2R using a non-peptide agonist called C21, on vascular function. Our results highlight that: 1) the physical interaction ("heterodimerization") between AT_2R and B_2R with MasR is necessary to exert the vasodilatory functions of the

protective arm of the RAS, 2) obesity interrupts that crosstalk, leading to a reduction of NO-dependent relaxation and 3) the activation of the AT_2R with C21 in obesity is sufficient to restore the interaction among the three receptors, activate the PKA/p-eNOS and the AKT/p-eNOS signaling pathways and restore the normal contractile/relaxant response in the thoracic aorta.

To determine the role of angiotensin receptors in obesity, we first analyzed the contractile and relaxant responses to Ang II in thoracic aorta rings. In the arteries from HF-C animals, Ang II caused a shift in the AT_1R-AT_2R equilibrium towards an AT_1R-mediated contraction, probably due to the relative abundance of this receptor as previously described by Jerez et al [38]. In fact, blockade of the dominating AT_1R with losartan unmasked the AT_2R-mediated relaxation, as it has been previously described in other models [39]. Interestingly, the independent blockade of AT_2R (with PD123177), B_2R (with HOE-140) or MasR (with A799) hindered the vasorelaxant responses to Ang II, even in the presence of C21 in lean animals. This effect, i.e. the inhibition of the downstream function of one receptor by antagonizing another receptor, is not exclusive for the RAS system, where it has been described for the AT_2R-MasR dimer [23,40], but also between the RAS and the β-adrenergic system [41] and others. Importantly, our findings indicate for the first time that this type of cross-regulation also occurs between the 2 members of the protective RAS and B_2R and it suggests a requirement for interaction among the three receptors to execute the actions of the protective arm of the RAS. In fact, obesity *per se* not only increased the contractile effects of Ang II as a result of AT_1R receptor overexpression as others have reported [42], but also through a disruption in the AT_2R/B_2R/MasR axis as evidenced by the lack of protective effects of these receptors in HF-C mice. Nevertheless, because of the low AT_{1b} receptor levels in the thoracic aorta compared to those observed in other arteries like the abdominal aorta

or the femoral artery [43], a limitation of this study is that thoracic contractile responses to Ang II, as well as the changes observed between groups, are small. Therefore, further research is needed to analyze if this obesity-induced increase in contractile response, although limited in magnitude, is a preliminary signal of vascular damage or if it has physiological relevance *per se*. That would help to further understand the protective effects of C21.

Interestingly, C21 was able to maintain the functionality of the thoracic aorta in obese animals by preserving AT_2R-mediated vasodilatory effects. It is noteworthy that this effect required an intact AT_2R/B_2R/MasR axis, since disruption of any of the three receptors abolished the effect.

Although several studies have shown the ability of AT_2R to form heterodimers with MasR and B_2R [44,45], our findings demonstrate for the first time the physical interaction among AT_2R/MasR and B_2R/MasR in endothelial cells. While MasR coimmunoprecipitated with both AT_2R and B_2R in untreated cells, this interaction was enhanced when the cells were treated with C21 likely due to increased expression of the 3 proteins both at the intracellular and membrane level. Furthermore, the glycosylated form of B_2R, which is required to promote its trafficking to the membrane, was also increased [46].

To shed some light on the endothelial damage caused by obesity, we analyzed the endothelium-dependent relaxant responses to ACh alone and in the presence of L-NAME to assess the net contribution of NO. Aortic rings from HF mice exhibited a significant reduction in ACh-induced relaxation due to an approximately 30% reduction in the availability of NO. It is known that obesity causes not only a reduction in the protein levels of eNOS in aorta [47,48] but also a decrease in phosphorylation of eNOS at Ser^{1777} [49,50]. The activation of AT_2R with C21 preserved NO levels in the aorta of obese

animals, in a mechanism that involves AKT-dependent Ser^{1777} phosphorylation of eNOS. It has also been described that the phosphatases downstream of AT_2R activation can dephosphorylate the inhibitory Tyr^{657} and Thr^{495} residues on eNOS [51].

Besides this direct mechanism of activation, C21 through AT_2R can also increase NO generation indirectly by triggering the activation of PKA/p-Ser^{663}eNOS [25,52]. In aortic rings from CHOW animals, there was a similar contribution of PKA/eNOS and AKT/eNOS signaling pathways in the generation of NO, that was completely abolished in obese mice but preserved by the treatment with C21. This complementary action of the two pathways was confirmed in endothelial cells, where each inhibitor independently reduced the NO release in response to C21 to half rate, and both together completely abrogated the C21-induced NO generation to basal levels. It has been already demonstrated that NO release can also result from AT_2R-mediated BK synthesis and the consequent activation of B_2R [53]. Therefore, and since BK levels were significantly increased in HECs treated with C21, a stimulation of BK synthesis by C21 cannot be discarded. Nevertheless, a limitation of this study is that murine aortic endothelial cell lines are not available, reason why *in vitro* studies were performed in HECs. Consequently, although we suggest that the results observed in HECs could explain the effects observed in the murine thoracic aorta, further studies should be required to clearly demonstrate it.

Further studies should be carried out to explore the nature of the desensitizing mechanisms that lead to disrupted physical interaction among AT_2R/B_2R/MasR in obesity. Although our data demonstrate the protein-protein interaction among the three receptors, we cannot disregard the possibility that C21 could also bind to the MasR based on structural similarities between the C21 and the MasR agonist, AVE 0991, although the region of the molecule critical for selective AT_2R binding is quite distinct

[40]. Nonetheless, even if C21 could stimulate AT_2R and MasR simultaneously, the use of one of the antagonists should only inhibit NO release partially instead of total ablation of the relaxant response, as we have found.

Altogether, the present data provide novel insights into a new premise regarding the activation of eNOS and the consequent NO release where, prior to the activation of the PKA/p-eNOS or the AKT/p-eNOS pathways, the combined action of the upstream heterodimers AT_2R/MasR and B_2R/MasR is required. Although in obesity, this crosstalk is interrupted, leading to a complete loss of the action of the protective arm of the RAS, we have shown that it can be restored with AT_2R stimulation.

Clinical Perspectives

- The reduction of nitric oxide availability lies in the basis of obesity-associated endothelial dysfunction. The stimulation of AT_2R by Compound 21 is known to induce NO release in endothelial cells, so the purpose of this study was to evaluate the effect of C21 on thoracic aorta endothelial function in a model of diet-induced obesity and to elucidate the implication of the potential crosstalk between AT_2R, MasR and/or B_2R in this response.
- This study evidences a defective AT_2R signaling due to the disruption of the AT_2R/B_2R/MasR axis associated to endothelial dysfunction in diet-induced obese mice. Chronic treatment with C21 prevents those alterations favoring AT_2R/MasR and B_2R/MasR heterodimerization, increased NO availability and vascular protection.
- C21, recognized as an orphan drug in idiopathic pulmonary fibrosis, is in phase II clinical trials for pulmonary fibrosis and COVID-19. Therefore, we suggest that activation of the renin-angiotensin system protective arm by C21 might constitute a

promising pharmacological strategy in the management of obesity-derived vascular damage.

Data availability statement: The data that support the findings of this study are available from the corresponding author upon reasonable request.

Funding: This work was supported by Fundación Universitaria San Pablo CEU – Santander; Ministerio de Economía y Competitividad (BFU2017-82565-C2-2-R); and Grupos Universidad Complutense de Madrid (GR-921641).

Acknowledgements: We thank J. M. Garrido, J. Bravo, and I. Bordallo for skillful animal care during the experiment. We thank Vicore Pharma for supplying Compound 21 required for this study.

Conflict of interest: none declared.

REFERENCES

1. World Health Organization. The top 10 causes of death. 2014. https://www.who.int/news-room/fact-sheets/detail/the-top-10-causes-of-death (18 September 2020)

2. Melgaard L, Gorst-Rasmussen A, Rasmussen LH, Lip GYH, Larsen TB. Vascular Disease and Risk Stratification for Ischemic Stroke and All-Cause Death in Heart Failure Patients without Diagnosed Atrial Fibrillation: A Nationwide Cohort Study. *PLoS One* PLoS One; 2016;**11**:e0152269.

3. García-Prieto CF, Gil-Ortega M, Vega-Martín E, Ramiro-Cortijo D, Martín-Ramos M, Bordiú E, Sanchez-Pernaute A, Torres A, Aránguez I, Fernández-Alfonso M, Rubio MA, Somoza B. Beneficial effect of bariatric surgery on abnormal MMP-9 and AMPK activities: Potential markers of obesity-related CV risk. *Front Physiol* Frontiers Media S.A.; 2019;**10**.

4. Gil-Ortega M, Condezo-Hoyos L, García-Prieto CF, Arribas SM, González MC, Aranguez I, Ruiz-Gayo M, Somoza B, Fernández-Alfonso MS. Imbalance between pro and anti-oxidant mechanisms in perivascular adipose tissue aggravates long-term high-fat diet-derived endothelial dysfunction. *PLoS One* Public Library of Science; 2014;**9**.

5. Gil-Ortega M, Martín-Ramos M, Arribas SM, González MC, Aránguez I, Ruiz-Gayo M, Somoza B, Fernández-Alfonso MS. Arterial stiffness is associated with adipokine dysregulation in non-hypertensive obese mice. *Vascul Pharmacol* Elsevier Inc.; 2016;**77**:38–47.

6. Arancibia-Radich J, González-Blázquez R, Alcalá M, Martín-Ramos M, Viana M, Arribas S, Delporte C, Fernández-Alfonso MS, Somoza B, Gil-Ortega M. Beneficial effects of murtilla extract and madecassic acid on insulin sensitivity and endothelial function in a model of diet-induced obesity. *Sci Rep* Nature Publishing Group; 2019;**9**.

7. Grassi G, Seravalle G, Scopelliti F, Dell'Oro R, Fattori L, Quarti-Trevano F, Brambilla G, Schiffrin EL, Mancia G. Structural and functional alterations of subcutaneous small resistance arteries in severe human obesity. *Obesity* Obesity (Silver Spring); 2010;**18**:92–98.

8. Arendse LB, Jan Danser AH, Poglitsch M, Touyz RM, Burnett JC, Llorens-Cortes C, Ehlers MR, Sturrock ED. Novel therapeutic approaches targeting the renin-angiotensin system and associated peptides in hypertension and heart failure. *Pharmacol Rev* American Society for Pharmacology and Experimental Therapy; 2019;**71**:539–570.

9. Nehme A, Zouein FA, Zayeri ZD, Zibara K. An Update on the Tissue Renin Angiotensin System and Its Role in Physiology and Pathology. *J Cardiovasc Dev Dis* MDPI AG; 2019;**6**:14.

10. Faloia E, Gatti C, Camilloni MA, Mariniello B, Sardu C, Garrapa GGM, Mantero F, Giacchetti G. Comparison of circulating and local adipose tissue renin-angiotensin system in normotensive and hypertensive obese subjects. *J Endocrinol Invest* J Endocrinol Invest; 2002;**25**:309–314.

11. Kawai T, Forrester SJ, O'Brien S, Baggett A, Rizzo V, Eguchi S. AT1 receptor signaling pathways in the cardiovascular system. Pharmacol. Res. Academic Press; 2017. p. 4–13.

12. Rincón J, Correia D, Arcaya JL, Finol E, Fernández A, Pérez M, Yaguas K, Talavera E, Chávez M, Summer R, Romero F. Role of Angiotensin II type 1 receptor on renal NAD(P)H oxidase, oxidative stress and inflammation in nitric oxide inhibition induced-hypertension. *Life Sci* Elsevier Inc.; 2015;**124**:81–90.

13. Li N, Wang HX, Han QY, Li WJ, Zhang YL, Du J, Xia YL, Li HH. Activation of the cardiac proteasome promotes angiotension II-induced hypertrophy by down-regulation of ATRAP. *J Mol Cell Cardiol* Academic Press; 2015;**79**:303–314.

14. Wang XP, Zhang R, Wu K, Wu L, Dong Y. Angiotensin II mediates acinar cell apoptosis during the development of rat pancreatic fibrosis by AT1R. *Pancreas* Pancreas; 2004;**29**:264–270.

15. Steckelings UM, Rompe F, Kaschina E, Namsolleck P, Grzesiak A, Funke-Kaiser H, Bader M, Unger T. The past, present and future of angiotensin II type 2 receptor stimulation. JRAAS - J. Renin-Angiotensin-Aldosterone Syst. J Renin Angiotensin Aldosterone Syst; 2010. p. 67–73.

16. Miura S ichiro, Matsuo Y, Kiya Y, Karnik SS, Saku K. Molecular mechanisms of the antagonistic action between AT1 and AT2 receptors. *Biochem Biophys Res Commun* Biochem Biophys Res Commun; 2010;**391**:85–90.

17. Forrester SJ, Booz GW, Sigmund CD, Coffman TM, Kawai T, Rizzo V, Scalia R, Eguchi S. Angiotensin II Signal Transduction: An Update on Mechanisms of Physiology and Pathophysiology. *Physiol Rev* American Physiological Society; 2018;**98**:1627–1738.

18. Tanaka M, Tsuchida S, Imai T, Fujii N, Miyazaki H, Ichiki T, Naruse M, Inagami T. Vascular response to angiotensin II is exaggerated through an upregulation of AT1 receptor in AT2 knockout mice. *Biochem Biophys Res Commun* Academic Press Inc.; 1999;**258**:194–198.

19. Cosentino F, Savoia C, Paolis P De, Francia P, Russo A, Maffei A, Venturelli V, Schiavoni M, Lembo G, Volpe M. Angiotensin II type 2 receptors contribute to vascular responses in spontaneously hypertensive rats treated with angiotensin II type 1 receptor antagonists. *Am J Hypertens* Elsevier Inc.; 2005;**18**:493–499.

20. Jin XQ, Fukuda N, Su JZ, Lai YM, Suzuki R, Tahira Y, Takagi H, Ikeda Y, Kanmatsuse K, Miyazaki H. Angiotensin II type 2 receptor gene transfer downregulates angiotensin II type 1a receptor in vascular smooth muscle cells. *Hypertension* Hypertension; 2002;**39**:1021–1027.

21. Inuzuka T, Fujioka Y, Tsuda M, Fujioka M, Satoh AO, Horiuchi K, Nishide S, Nanbo A, Tanaka S, Ohba Y. Attenuation of ligand-induced activation of angiotensin II type 1 receptor signaling by the type 2 receptor via protein kinase C. *Sci Rep* Nature Publishing Group; 2016;**6**.

22. AbdAlla S, Lother H, Abdel-tawab AM, Quitterer U. The Angiotensin II AT2 Receptor Is an AT1 Receptor Antagonist. *J Biol Chem* J Biol Chem; 2001;**276**:39721–39726.

23. Leonhardt J, Villela DC, Teichmann A, Münter LM, Mayer MC, Mardahl M, Kirsch S, Namsolleck P, Lucht K, Benz V, Alenina N, Daniell N, Horiuchi M, Iwai M, Multhaup G, Schülein R, Bader M, Santos RA, Unger T, Steckelings UM. Evidence for Heterodimerization and Functional Interaction of the Angiotensin Type 2 Receptor and the Receptor MAS. *Hypertension* Lippincott Williams and Wilkins; 2017;**69**:1128–1135.

24. Abadir PM, Periasamy A, Carey RM, Siragy HM. Angiotensin II type 2 receptor-bradykinin B2 receptor functional heterodimerization. *Hypertension* Hypertension; 2006;**48**:316–322.

25. Gohlke P, Pees C, Unger T. AT2 Receptor Stimulation Increases Aortic Cyclic GMP in SHRSP by a Kinin-Dependent Mechanism. *Hypertension* Hypertension; 1998;**31**:349–355.

26. Kalupahana NS, Moustaid-Moussa N. The renin-angiotensin system: A link between obesity, inflammation and insulin resistance. Obes. Rev. Obes Rev; 2012. p. 136–149.

27. Gatineau E, Gong MC, Yiannikouris F. Soluble Prorenin Receptor Increases Blood Pressure in High Fat-Fed Male Mice. *Hypertension* Lippincott Williams and Wilkins; 2019;**74**:1014–1020.

28. Kaschina E, Namsolleck P, Unger T. AT2 receptors in cardiovascular and renal diseases. Pharmacol. Res. Academic Press; 2017. p. 39–47.

29. Hagihara GN, Lobato NS, Filgueira FP, Akamine EH, Aragão DS, Casarini DE, Carvalho MHC, Fortes ZB. Upregulation of ERK1/2-eNOS via AT2 receptors decreases the contractile response to angiotensin II in resistance mesenteric arteries from obese rats. *PLoS One* PLoS One; 2014;**9**.

30. Karpe PA, Gupta J, Marthong RF, Ramarao P, Tikoo K. Insulin resistance induces a segmental difference in thoracic and abdominal aorta: Differential expression of AT1 and AT2 receptors. *J Hypertens* Lippincott Williams and Wilkins; 2012;**30**:132–146.

31. González-Blázquez R, Somoza B, Gil-Ortega M, Ramos MM, Ramiro-Cortijo D, Vega-Martín E, Schulz A, Ruilope LM, Kolkhof P, Kreutz R, Fernández-Alfonso MS. Finerenone attenuates endothelial dysfunction and albuminuria in a chronic kidney disease model by a reduction in oxidative stress. *Front Pharmacol* Frontiers Media S.A.; 2018;**9**.

32. Somoza B, Guzmán R, Cano V, Merino B, Ramos P, Díez-Fernández C, Fernández-Alfonso MS, Ruiz-Gayo M. Induction of cardiac uncoupling protein-2 expression and adenosine 5′-monophosphate-activated protein kinase phosphorylation during early states of diet-induced obesity in mice. *Endocrinology* Endocrinology; 2007;**148**:924–931.

33. Li Q, Lau A, Morris TJ, Guo L, Fordyce CB, Stanley EF. A Syntaxin 1, Gαo, and N-Type Calcium Channel Complex at a Presynaptic Nerve Terminal: Analysis by Quantitative Immunocolocalization. *J Neurosci* J Neurosci; 2004;**24**:4070–4081.

34. Juarez E, Tufiño C, Querejeta E, Bracho-Valdes I, Bobadilla-Lugo RA. Evidence of changes in alpha-1/AT1 receptor function generated by diet-induced obesity. *Diabetes Vasc Dis Res* SAGE Publications Ltd; 2017;**14**:485–493.

35. Madrigal Aguilar DA, Tufiño C, Fernandez-Martinez E, Bracho-Valdés I, Bobadilla Lugo RA. AT1R antagonism improves metabolic and vascular changes of obesity-induced gestational diabetes mellitus. *Pathophysiology* Elsevier B.V.; 2019;**26**:121–127.

36. Schinzari F, Tesauro M, Veneziani A, Mores N, Daniele N Di, Cardillo C. Favorable Vascular Actions of Angiotensin-(1-7) in Human Obesity. *Hypertension* Lippincott Williams and Wilkins; 2018;**71**:185–191.

37. Nag S, Patel S, Mani S, Hussain T. Role of angiotensin type 2 receptor in improving lipid metabolism and preventing adiposity. *Mol Cell Biochem* Springer New York LLC; 2019;**461**:195–204.

38. Jerez S, Scacchi F, Sierra L, Karbiner S, Peral De Bruno M. Vascular hyporeactivity to angiotensin II and noradrenaline in a rabbit model of obesity. *J Cardiovasc Pharmacol* J Cardiovasc Pharmacol; 2012;**59**:49–57.

39. Gennaro Colonna V De, Rigamonti A, Fioretti S, Bonomo S, Manfredi B, Ferrario P, Bianchi M, Berti F, Muller EE, Rossoni G. Angiotensin-converting enzyme inhibition and angiotensin AT1-receptor antagonism equally improve endothelial vasodilator function in L-NAME-induced hypertensive rats. *Eur J Pharmacol* 2005;**516**:253–259.

40. Villela D, Leonhardt J, Patel N, Joseph J, Kirsch S, Hallberg A, Unger T, Bader M, Santos RA, Sumners C, Steckelings UM. Angiotensin type 2 receptor (AT2R) and receptor Mas: A complex liaison. *Clin Sci* Portland Press Ltd; 2015;**128**:227–234.

41. Barki-Harrington L, Luttrell LM, Rockman HA. Dual inhibition of β-adrenergic and angiotensin II receptors by a single antagonist: A functional role for receptor-receptor interaction in vivo. *Circulation* Circulation; 2003;**108**:1611–1618.

42. Kim JI. High fat diet confers vascular hyper-contractility against angiotensin II through upregulation of MLCK and CPI-17. *Korean J Physiol Pharmacol* Korean Physiological Soc. and Korean Soc. of Pharmacology; 2017;**21**:99–106.

43. Zhou Y, Dirksen WP, Babu GJ, Periasamy M. Differential vasoconstrictions induced by angiotensin II: role of AT1 and AT2 receptors in isolated C57BL/6J mouse blood vessels. *Am J Physiol Circ Physiol* American Physiological Society; 2003;**285**:H2797–H2803.

44. Lyngsø C, Erikstrup N, Hansen JL. Functional interactions between 7TM receptors in the Renin-Angiotensin System-Dimerization or crosstalk? Mol. Cell. Endocrinol. Mol Cell Endocrinol; 2009. p. 203–212.

45. Patel SN, Ali Q, Samuel P, Steckelings UM, Hussain T. Angiotensin II type 2 receptor and receptor mas are colocalized and functionally interdependent in obese zucker rat kidney. *Hypertension* Lippincott Williams and Wilkins; 2017;**70**:831–838.

46. Michineau S, Muller L, Pizard A, Alhenc-Gélas F, Rajerison RM. N-linked glycosylation of the human bradykinin B2 receptor is required for optimal cell-surface expression and coupling. *Biol Chem* Biol Chem; 2004;**385**:49–57.

47. Yang N, Ying C, Xu M, Zuo X, Ye X, Liu L, Nara Y, Sun X. High-fat diet up-

regulates caveolin-1 expression in aorta of diet-induced obese but not in diet-resistant rats. *Cardiovasc Res* Oxford Academic; 2007;**76**:167–174.

48. Georgescu A, Popov D, Constantin A, Nemecz M, Alexandru N, Cochior D, Tudor A. Dysfunction of human subcutaneous fat arterioles in obesity alone or obesity associated with Type 2 diabetes. *Clin Sci* Portland Press; 2011;**120**:463–472.

49. Kim F, Pham M, Maloney E, Rizzo NO, Morton GJ, Wisse BE, Kirk EA, Chait A, Schwartz MW. Vascular inflammation, insulin resistance, and reduced nitric oxide production precede the onset of peripheral insulin resistance. *Arterioscler Thromb Vasc Biol* NIH Public Access; 2008;**28**:1982–1988.

50. Naruse K, Rask-Madsen C, Takahara N, Ha SW, Suzuma K, Way KJ, Jacobs JRC, Clermont AC, Ueki K, Ohshiro Y, Zhang J, Goldfine AB, King GL. Activation of vascular protein kinase C-beta; inhibits Akt-dependent endothelial nitric oxide synthase function in obesity-associated insulin resistance. *Diabetes* American Diabetes Association Inc.; 2006;**55**:691–698.

51. Augusto Peluso A, Bertelsen JB, Andersen K, Mortsensen TP, Hansen PB, Sumners C, Bader M, Santos RA, Steckelings UM. Identification of protein phosphatase involvement in the AT2 receptor-induced activation of endothelial nitric oxide synthase. *Clin Sci* Portland Press Ltd; 2018;**132**:777–790.

52. Iring A, Jin YJ, Albarrán-Juárez J, Siragusa M, Wang SP, Dancs PT, Nakayama A, Tonack S, Chen M, Künne C, Sokol AM, Günther S, Martínez A, Fleming I, Wettschureck N, Graumann J, Weinstein LS, Offermanns S. Shear stress-induced endothelial adrenomedullin signaling regulates vascular tone and blood pressure. *J Clin Invest* American Society for Clinical Investigation; 2019;**129**:2775–2791.

53. Abadir PM, Carey RM, Siragy HM. Angiotensin AT2 receptors directly stimulate renal nitric oxide in Bradykinin B2-receptor-null mice. *Hypertension* Hypertension; 2003;**42**:600–604.

FIGURE LEGENDS

Figure 1. Characterization of contractile and relaxant responses to Ang II: role of AT_2R, MasR and B_2R. Cumulative concentration-response curves to Ang II (10^{-9}-10^{-6} mol/l) in aortic segments from (A) CHOW and HF animals treated or not with C21, (B-E) CHOW-C (B), CHOW-C21 (C), HF-C (D) and HF-C21 (E) mice pre-incubated or not with PD123177, A-779 or HOE-140. Cumulative concentration-response curves to Ang II (10^{-9}-10^{-6} mol/l) in aortic segments pre-incubated with losartan (10^{-7} mol/l) from (F) CHOW and HF animals treated or not with C21, (G-J) CHOW-C (G), CHOW-C21 (H), HF-C (I) and HF-C21 (J) pre-incubated or not with PD123177, A-779 or HOE-140. Results are represented as the mean ± S.E.M. (n = 10). (A and F) **p<0.01 and ***p<0.001 compared with CHOW-C mice; $^{\#\#}$p<0.01 and $^{\#\#\#}$p<0.001 compared with HF-C mice. (B-E and G-J) *p<0.05 and **p<0.01 PD123177 *vs* C, $^{\#}$p<0.05, $^{\#\#}$p<0.01 and $^{\#\#\#}$p<0.001 A779 *vs* C and $^{\&}$p<0.05 HOE-140 *vs* C. (2-ANOVA; Bonferroni post hoc test).

Figure 2. Characterization of the interaction between AT_2R, MasR and B_2R.

(A) Co-immunoprecipitation (Co-IP) of AT_2R, MasR and B_2R heterodimers in HECs. The Co-IP lanes represent proteins immunoprecipitated with the MasR antibody attached to protein A/G PLUS-Agarose. Co-immunoprecipitants (IP) were analyzed by SDS-PAGE and immunoblotted (IB) using the indicated antibodies. These blots are representative of AT_2R, MasR, B_2R and α-tubulin expression in samples from HECs treated or not with C21. The Input lanes represent immunoblot analysis of cell extracts before immunoprecipitation. NS, non-specific, refers to omission of the primary antibody in the Co-IP assay. (B) Densitometric analysis of the MasR-AT_2R and (C) MasR-B_2R heterodimers. Equal amounts of proteins were IP with the MasR antibody and IB with the AT_2R and B_2R antibody, respectively. The IP signal was normalized

against the input bands. Results are expressed relative to control and represented as the mean ± S.E.M of a minimum of 5 independent experiments. *p<0.05, compared with C (Student's t-test). (D-E) Representative confocal projections of HECs treated or not with C21 and stained with anti-AT_2R (red) and (C) anti-MasR or (D) anti-B_2R (green) antibodies. Nuclei staining was performed with DAPI (blue). (F-H) Dot plot graphs show quantification of fluorescence intensity for AT_2R (F), MasR (G) and B_2R (H). Results are represented as the mean ± S.E.M. (n = 6). *p<0.05 compared with C (Student's t-test).

Figure 3. Effect of C21 treatment on obesity-derived endothelial dysfunction and NO availability. Cumulative concentration-response curves to ACh (10^{-9}-10^{-4} mol/l) in aortic segments from (A) CHOW and HF animals treated or not with C21, (B- E) CHOW-C (B), CHOW-C21 (C), HF-C (D) and HF-C21 (E) animals pre-incubated or not with L-NAME (10^{-4} mol/l). Results are represented as the mean ± S.E.M. (n = 7 - 10). (A) ***p<0.001 compared with CHOW-C mice; $^{###}$p<0.001 compared with HF-C mice. (B-E) ***p<0.001 compared with their corresponding matched control groups. (2-ANOVA; Bonferroni post hoc test). (F) AUC, Area under concentration–response curves elicited by ACh in presence (black bars) or absence (full histogram) of L-NAME. AUC is expressed in arbitrary units. White bars represent the difference between the AUC in presence and absence of L-NAME. **p<0.01 and ***p<0.001 (1-ANOVA; Bonferroni post hoc test).

Figure 4. Role of AT_2R, MasR and B_2R in NO production. (A) Representative immunoblots of p-eNOS^{Ser1177}/eNOS and b-actin expression in HECs previously incubated or not with PD123177, A-779 or HOE-140 and treated or not with C21. Bars graph shows the result of densitometric analysis of p-eNOS^{Ser1177}/eNOS immunoblots expressed as percentage of p-eNOS^{Ser1177}/eNOS in C HECs. (B) Representative pictures

of HECs previously incubated or not with PD123177, A-779 or HOE-140 and treated with C21 or nothing as control and incubated with DAF-2 DA (green). Nuclei staining was performed with DAPI (blue). (C) Dot plot graphs show quantification of fluorescence intensity with DAF-2. Results are represented as the mean ± S.E.M. (n = 5-7). ***p<0.001 compared with C; $^{\#\#}$p<0.01 and $^{\#\#\#}$p<0.001 compared with C21 (1-ANOVA; Bonferroni post hoc test).

Figure 5. Characterization of signaling pathways involved in C21-mediated NO release. Cumulative concentration-response curves to Ang II (10^{-9}-10^{-6} mol/l) in aortic segments from CHOW-C (A), CHOW-C21 (B), HF-C (C) and HF-C21 (D) mice pre-incubated with losartan (10^{-7} mol/l) and with KT-5720, triciribine or untreated as control. (E, F) AUC, Area under concentration–response curves elicited by ACh in presence (black bars) or absence (full histogram) of KT-5720 (E) or triciribine (F). White bars represent the difference between the AUC in presence and absence of KT-5720 or triciribine. AUC is expressed in arbitrary units. Results are represented as the mean ± S.E.M. (n = 10). *p<0.05 and **p<0.01 KT-5720 *vs* C; $^{\#}$p<0.05 and $^{\#\#}$p<0.01 triciribine *vs* C. (1-ANOVA; Bonferroni post hoc test).

Figure 6. Implication of PKA/eNOS and AKT/eNOS signaling pathways in NO production. (A) Representative pictures of HECs previously incubated or not with KT-5720 or triciribine, treated or not with C21 and incubated with DAF-2 DA (green). Nuclei staining was performed with DAPI (blue). (B) Dot plot graphs show quantification of fluorescence intensity with DAF-2. Results are represented as the mean ± S.E.M. (n = 5). *p<0.05, **p<0.01 and ***p<0.001 compared with C; $^{\#\#\#}$p<0.001 compared with C21 (1-ANOVA; Bonferroni post hoc test).

Figure 7. Mechanisms involved in NO release mediated by AT_2R stimulation with C21.

C21 favors a crosstalk between AT_2R, MasR and B_2R, leading to i) an increased BK release and its consequent activation of B_2R and ii) the activation of both PKA/eNOS and AKT/eNOS signaling pathways, thus enhancing NO release and contributing to vascular protection.

Figure 1

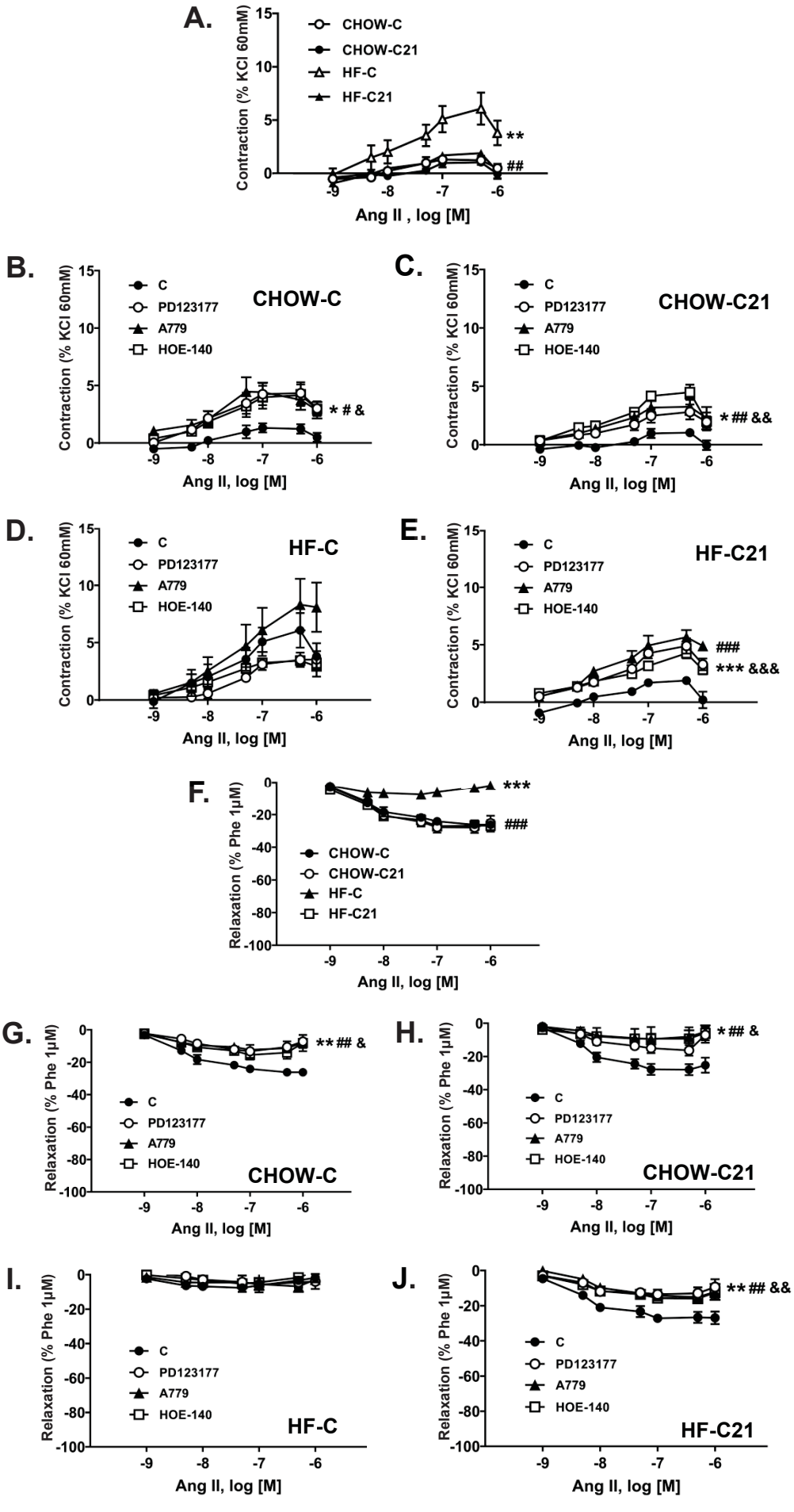
A.
CHOW-C
CHOW-C21
HF-C
HF-C21
Contraction (% KCl 60mM)
Ang II , log [M]
**
##
B.
CHOW-C
C
PD123177
A779
HOE-140
Contraction (% KCl 60mM)
Ang II, log [M]
* # &
C.
CHOW-C21
* ## &&
D.
HF-C
E.
HF-C21
###
*** &&&
F.
Relaxation (% Phe 1µM)
***
###
G.
** ## &
H.
* ## &
I.
J.
** ## &&

Figure 2

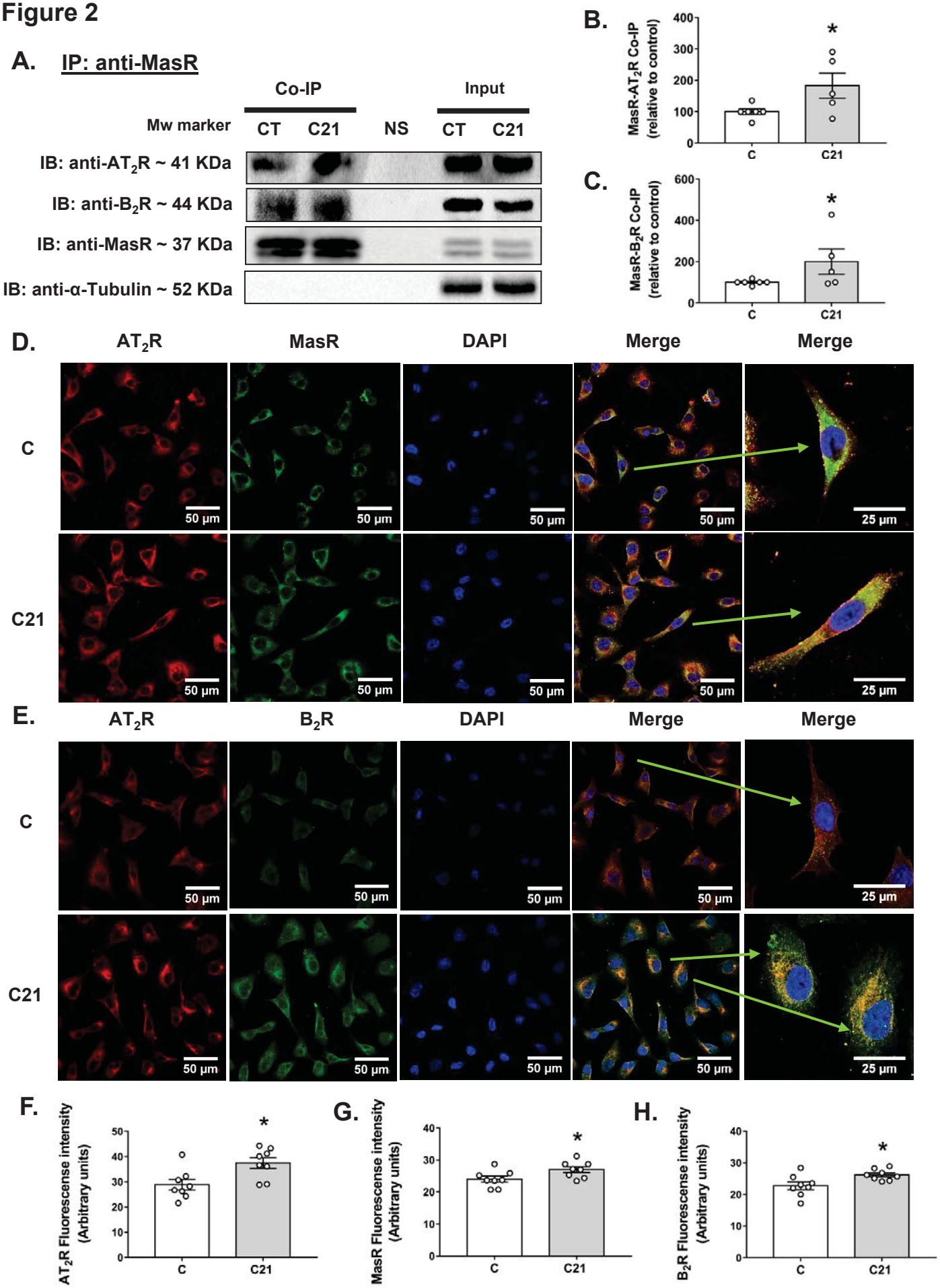
A.
IP: anti-MasR
Co-IP
Input
Mw marker
CT
C21
NS
CT
C21
IB: anti-AT2R ~ 41 KDa
IB: anti-B2R ~ 44 KDa
IB: anti-MasR ~ 37 KDa
IB: anti-α-Tubulin ~ 52 KDa
B.
MasR-AT2R Co-IP (relative to control)
400
300
200
100
0
C
C21
C.
MasR-B2R Co-IP (relative to control)
600
400
200
0
C
C21
D.
AT2R
MasR
DAPI
Merge
Merge
C
C21
50 µm
25 µm
E.
AT2R
B2R
DAPI
Merge
Merge
C
C21
50 µm
25 µm
F.
AT2R Fluorescense intensity (Arbitrary units)
50
40
30
20
10
0
C
C21
G.
MasR Fluorescense intensity (Arbitrary units)
40
30
20
10
0
C
C21
H.
B2R Fluorescense intensity (Arbitrary units)
40
30
20
10
0
C
C21

Figure 3

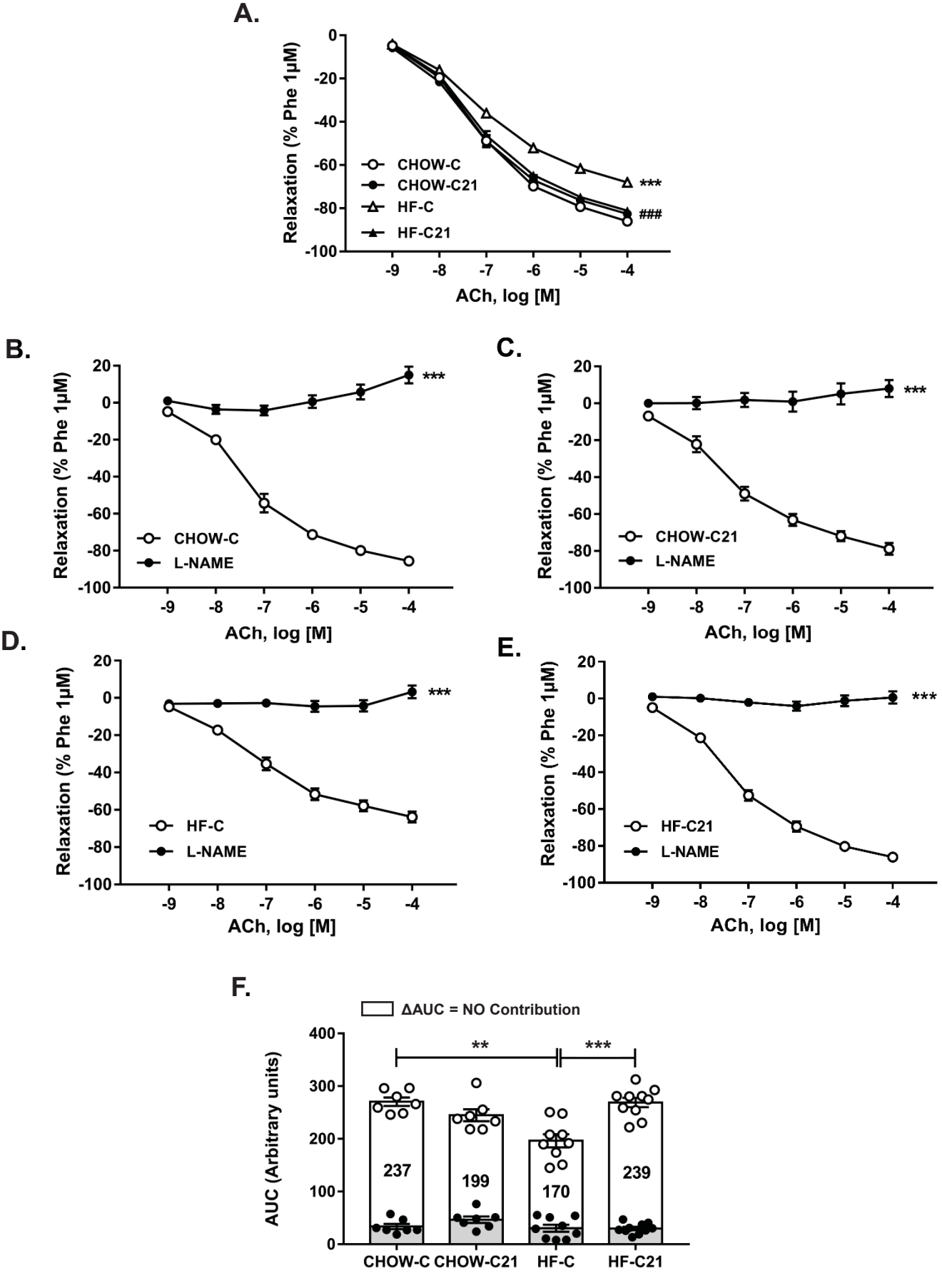
A.
Relaxation (% Phe 1µM)
0
-20
-40
-60
-80
-100
CHOW-C
CHOW-C21
HF-C
HF-C21
***
###
-9
-8
-7
-6
-5
-4
ACh, log [M]
B.
Relaxation (% Phe 1µM)
20
0
-20
-40
-60
-80
-100
CHOW-C
L-NAME
***
-9
-8
-7
-6
-5
-4
ACh, log [M]
C.
Relaxation (% Phe 1µM)
20
0
-20
-40
-60
-80
-100
CHOW-C21
L-NAME
***
-9
-8
-7
-6
-5
-4
ACh, log [M]
D.
Relaxation (% Phe 1µM)
20
0
-20
-40
-60
-80
-100
HF-C
L-NAME
***
-9
-8
-7
-6
-5
-4
ACh, log [M]
E.
Relaxation (% Phe 1µM)
20
0
-20
-40
-60
-80
-100
HF-C21
L-NAME
***
-9
-8
-7
-6
-5
-4
ACh, log [M]
F.
ΔAUC = NO Contribution
AUC (Arbitrary units)
400
300
200
100
0
**
***
237
199
170
239
CHOW-C
CHOW-C21
HF-C
HF-C21

Figure 4

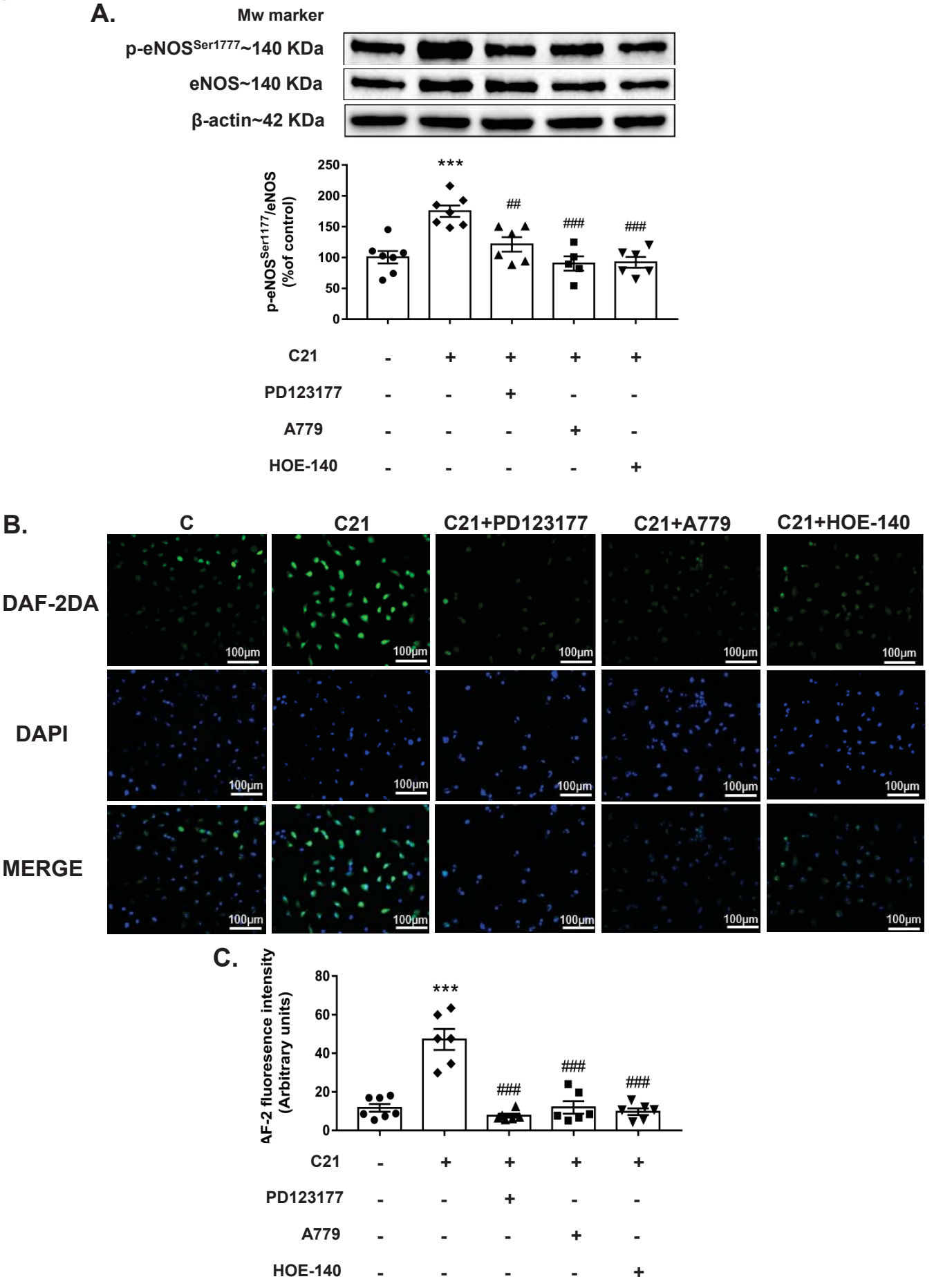
A.
Mw marker
p-eNOS^{Ser1777}~140 KDa
eNOS~140 KDa
β-actin~42 KDa
p-eNOS^{Ser1177}/eNOS (%of control)
250
200
150
100
50
0
***
##
###
###
C21 - + + + +
PD123177 - - + - -
A779 - - - + -
HOE-140 - - - - +
B.
C
C21
C21+PD123177
C21+A779
C21+HOE-140
DAF-2DA
DAPI
MERGE
100μm
C.
DAF-2 fluoresence intensity (Arbitrary units)
80
60
40
20
0
***
###
###
###
C21 - + + + +
PD123177 - - + - -
A779 - - - + -
HOE-140 - - - - +

Figure 5

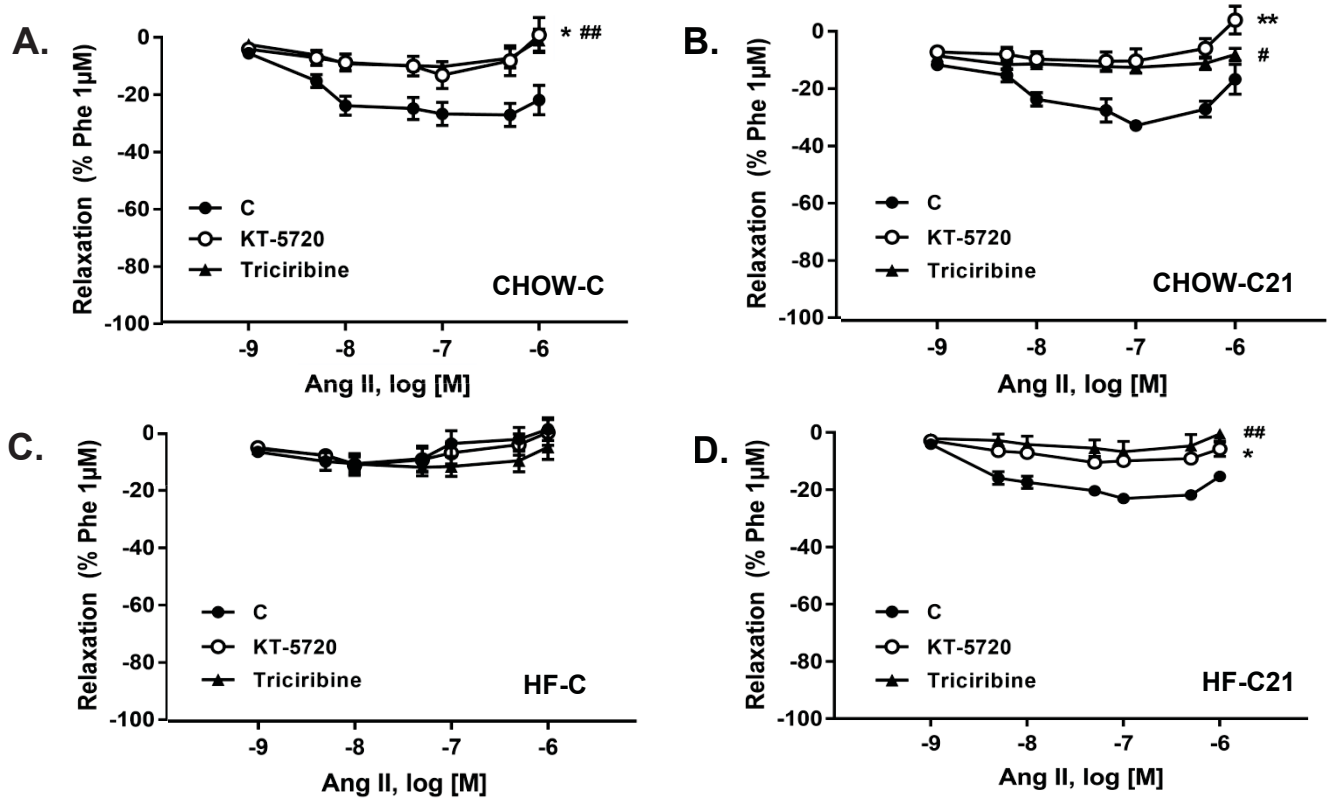
A.
B.
C.
D.
Relaxation (% Phe 1µM)
Ang II, log [M]
C
KT-5720
Triciribine
CHOW-C
CHOW-C21
HF-C
HF-C21
* ##
**
#
##
*

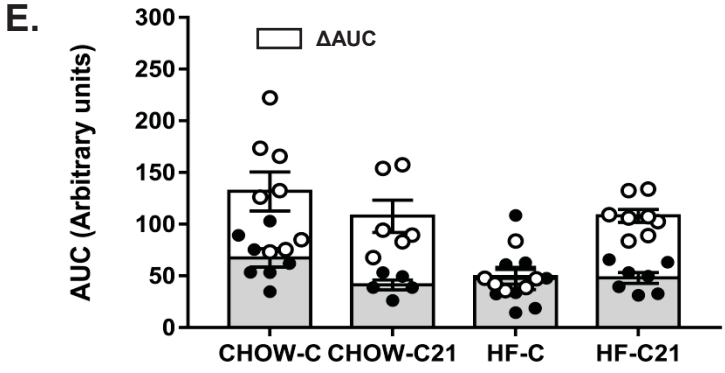
E.
AUC (Arbitrary units)
ΔAUC
CHOW-C
CHOW-C21
HF-C
HF-C21

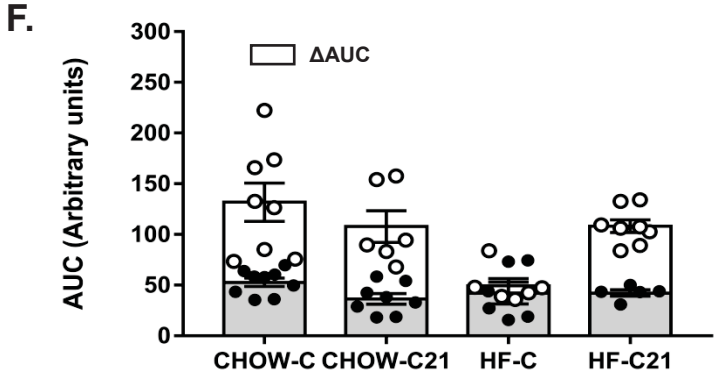
F.
AUC (Arbitrary units)
ΔAUC
CHOW-C
CHOW-C21
HF-C
HF-C21

Figure 6

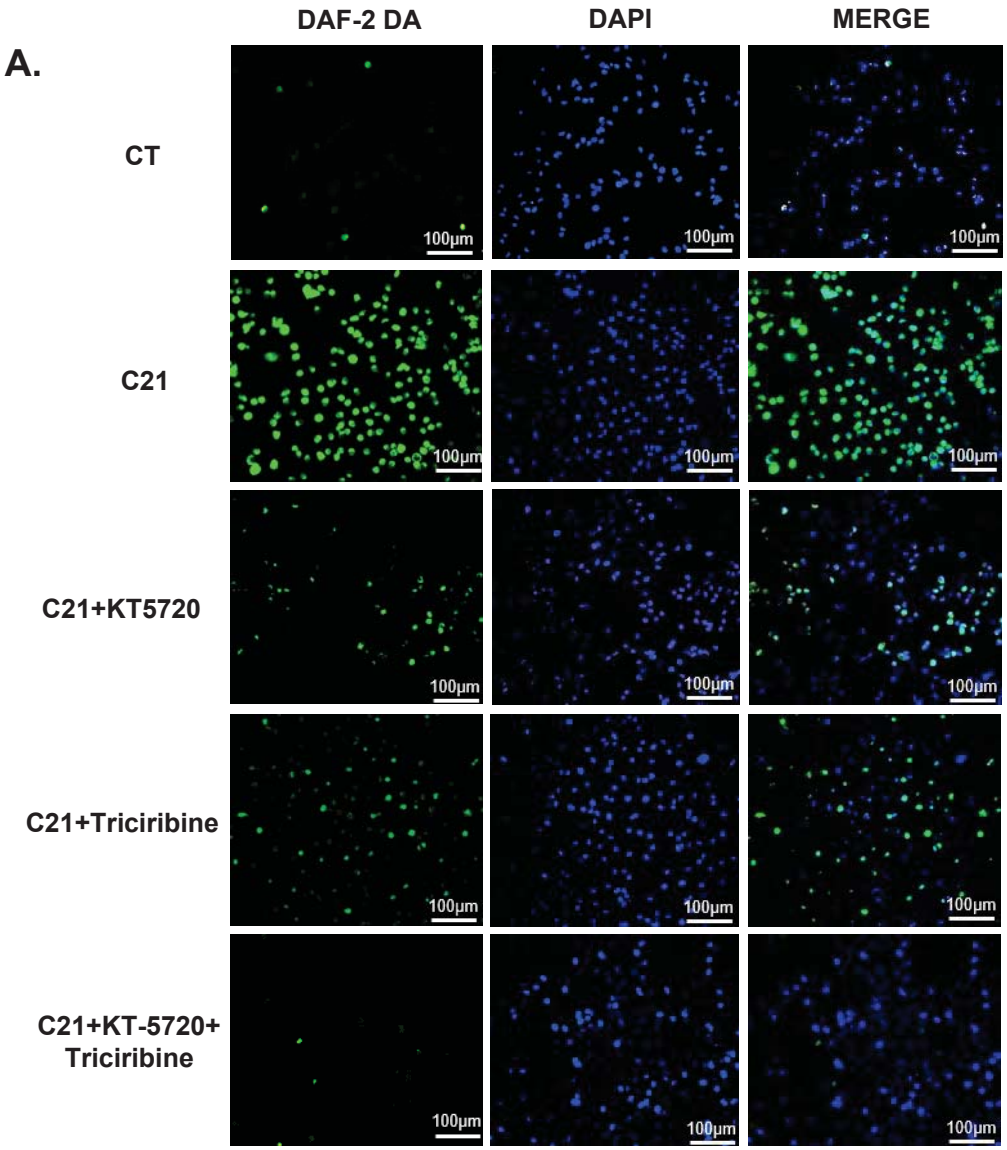
A.
DAF-2 DA
DAPI
MERGE
CT
C21
C21+KT5720
C21+Triciribine
C21+KT-5720+
Triciribine
100μm

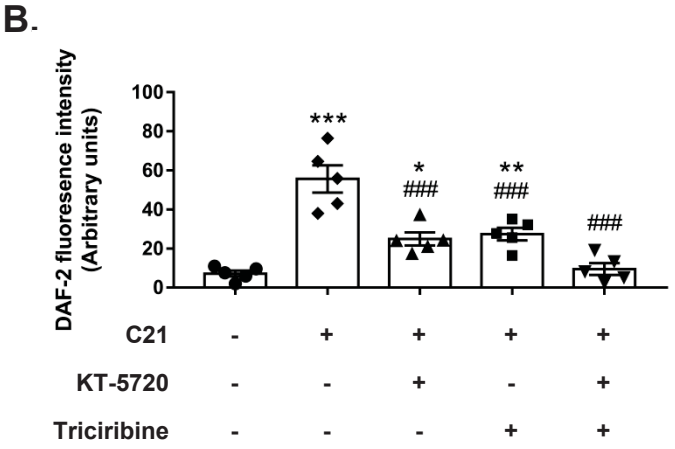
B.
DAF-2 fluorescence intensity
(Arbitrary units)
100
80
60
40
20
0
***
*
###
**
###
###
C21 - + + + +
KT-5720 - - + - +
Triciribine - - - + +

Figure 7

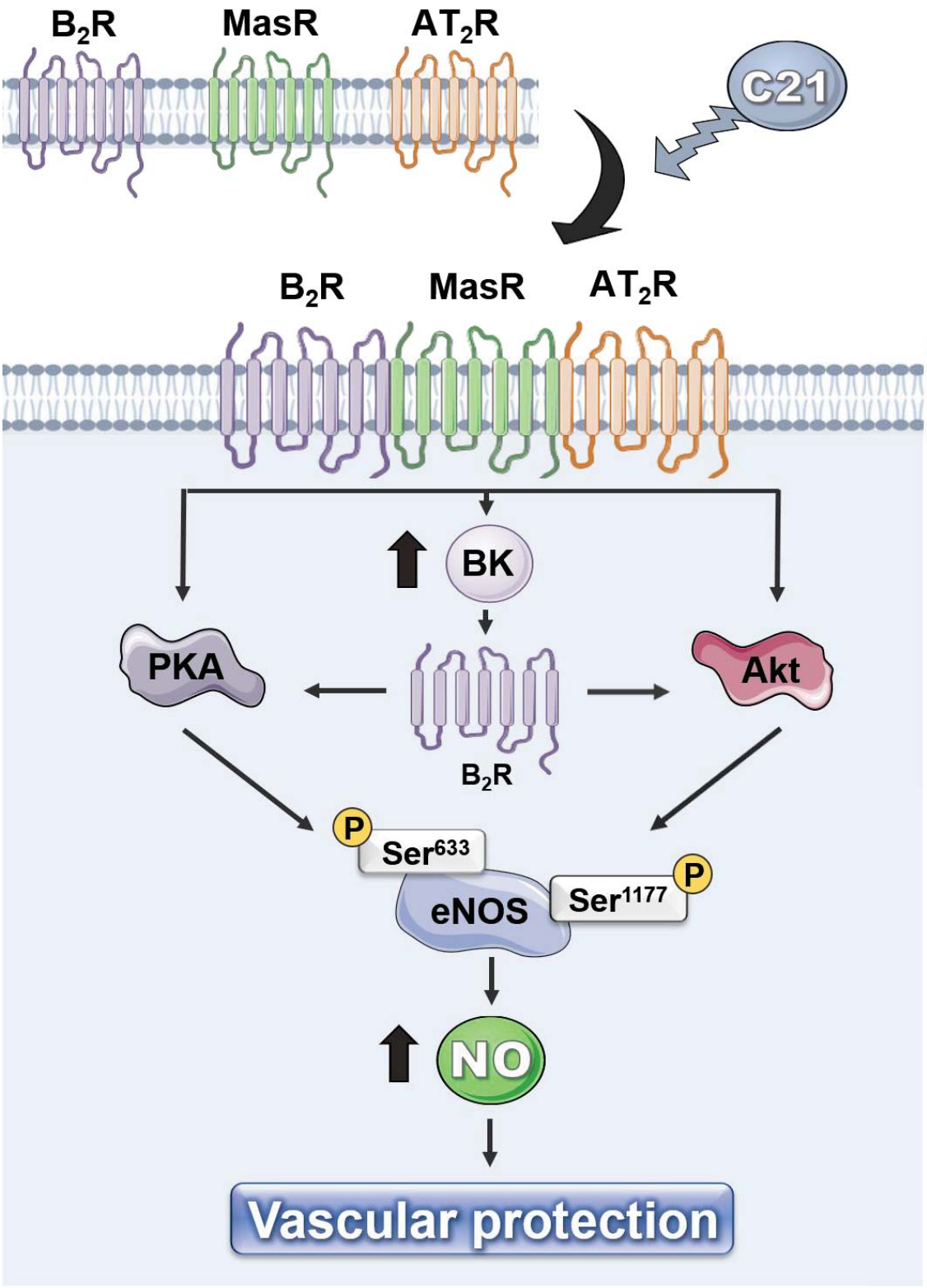
B2R
MasR
AT2R
C21
B2R
MasR
AT2R
BK
PKA
Akt
B2R
P
Ser633
eNOS
Ser1177
P
NO
Vascular protection

Table 1. Effect of diet and treatment with C21 on body weight and biochemical parameters.

	CHOW-C	CHOW-C21	HF-C	HF-C21
Body weight (g)	26.7 ± 1.0	26.8 ± 0.7	31.3 ± 1.5*	34.0 ± 1.7**
Biochemical parameters:				
Plasma glucose (mg/dL)	183.4 ± 1.4	175.2 ± 5.5	196.7 ± 2.6*	198.5 ± 2.2*
Plasma insulin (μg/L)	0.6 ± 0.1	1.2 ± 0.2	3.5 ± 0.4***	2.2 ± 0.2$^{\#}$
Plasma TG (mg/dL)	135.7 ± 11.7	135.0 ± 12.2	111.4 ± 9.4	117.1 ± 9.6
Plasma cholesterol (mg/dL)	98.9 ± 3.8	101.6 ± 2.9	148.1 ± 3.9***	149.8 ± 2.4***
Plasma NEFA (mM)	0.6 ± 0.04	0.7 ± 0.1	0.6 ± 0.03	0.5 ± 0.03$^{\#}$

Data are expressed as mean ± SEM (n = 5-10 determinations per group). *p<0.05, **p<0.01 and ***p<0.001 *vs* Chow-C mice; $^{\#}$p<0.05 *vs* HF-C mice (1-ANOVA; Bonferroni post hoc test). Triglycerides (TG), non-esterified fatty acid (NEFA).

Table 2. Co-localization analyses.

	Control	C21
AT_2R-MasR		
PCC (Rr)	0,77 ± 0,02	0,78 ± 0,01
MOC (R)	0,78 ± 0,01	0,80 ± 0,01
AT_2R – B_2R		
PCC (Rr)	0,65 ± 0,03	0,69 ± 0,03
MOC (R)	0,67 ± 0,06	0,67 ± 0,03

Data are expressed as mean ± SEM (n = 6). Pearson correlation coefficient (PCC); Mander's overlap coefficient (MOC).